Supplementary material for [Alasdair Bulloch, Shaoyang Wang, Paheli Ghosh, Lethy Krishnan Jagadamma], [2021], [Hysteresis in Hybrid Perovskite Indoor Photovoltaics], *Phil. Trans. R. Soc. A.*
doi: 10.1098/rsta.[paper ID in form xxxx.xxxx e.g. 10.1098/rsta.2014.0049]

Hysteresis in Hybrid Perovskite Indoor Photovoltaics

Experimental methods

(a) Fabrication of perovskite photovoltaic devices

Materials

The chemicals used to prepare the $MAPbI_3$ and $Cs_{0.05}FA_{0.81}MA_{0.14}PbI_{2.55}Br_{0.45}$ triple cation (TCA) perovskite precursor solution, MAI, MABr and FAI were used as received from Greatcell solar, PbI_2, $PbBr_2$ and CsI [99.999% purity] were bought from Alfa Aesar. The same CsI and $PbBr_2$, [99.999% purity] was used for preparation of $CsPbIBr_2$ perovskite solution. The SnO_2 solution (CAS 18282-10-5) for the electron transport layer (ETL) was bought from Alfa Aesar and diluted to the volume ratio 1:6.5 in deionized (DI) water prior to spin coating. The materials used for hole transport layer (HTL) solution preparation [2,2′,7,7′-Tetrakis[N,N-di(4-methoxyphenyl)amino]-9,9′-spirobiflourene (Spiro-OMeTAD, >99% purity), 4-tert-butyl pyridine (tBP, 96% purity), lithium-bis(tri-fluoromethanesulfonyl)imide (Li-TFSI, 99.95% purity) and tris(2-(1H-pyrazol-1-yl)-4-tert-butylpyridine)cobalt(III) tri[bis(trifluoromethane)sulfonimide] (FK 209) were purchased from Ossila, Sigma Aldrich and Greatcell Solar Materials, respectively. For p-i-n devices, bathocuproine (BCP) was acquired from Sigma Aldrich (99.99% purity), $PC_{60}BM$ and poly(4-butyltriphenylamine) (poly-TPD) from American Dye Source Inc., and poly[(9,9-bis(3'-(N,N-dimethylamino)propyl)-2,7-fluorene)-alt-2,7-(9,9-dioctylfluorene) (PFN) was bought from 1 Materials. Solvents dimethyl sulfoxide (DMSO, anhydrous, ≥99.9%), N,N-dimethylformamide (DMF, anhydrous, 99.8%), chlorobenzene (anhydrous, 99.8%), acetonitrile (anhydrous, 99.8%), and diethyl ether (anhydrous, ≥99.7%) were purchased from Sigma Aldrich.

Device fabrication

For n-i-p devices, patterned indium tin oxide (ITO)-coated glass substrates (glass/ITO with a sheet resistance of 15 $\Omega\ \square^{-1}$) were sequentially cleaned with sodium dodecyl sulphate (SDS), deionized water, acetone and isopropyl alcohol followed by plasma cleaning for 3 minutes with oxygen plasma in a Plasma Asher. A compact hole-blocking SnO_2 ETL was spin-coated using 100 μL of SnO_2 solution [diluted to 1:6.5 volume ratio in DI water] at 3000 rpm for 30 seconds, followed by thermal annealing at 150°C for 30 minutes on a hot plate in ambient conditions inside a laminar flow fume hood. For the $Cs_{0.05}FA_{0.81}MA_{0.14}PbI_{2.55}Br_{0.45}$ TCA perovskite solution, FAI (0.97M; 167 mg), PbI_2 (1.013 M; 467 mg), MABr (0.17 M; 19 mg), $PbBr_2$ (0.185 M; 68 mg), and CsI (0.061 M, 16 mg) were dissolved in a 1 mL

mixture of anhydrous DMF and DMSO (volume ratio 4:1) and stirred continuously for 1 hour. The TCA precursor solution was spin-coated on top of the SnO_2 ETL using two-step spin-coating, the first step at 1000 rpm for 10 seconds followed by a second step at 6000 rpm for 20 seconds. 90 µL of the TCA mixed halide solution was used for spin coating of the perovskite layer which was then treated with 250 µL of chlorobenzene as anti-solvent during the last 6th second of the second spin coating step. These films were then annealed at 100°C on a hot plate for 1 hour. Preparation of the $CsPbBr_2I$ perovskite solution involved using CsI (1 M; 259.8 mg) and $PbBr_2$ (1 M; 367.01 mg) as precursor materials, dissolved in anhydrous DMSO (1 mL) and continuous stirring for 2 hours at room temperature to achieve the desire $CsPbIBr_2$ composition. The $CsPbIBr_2$ perovskite solution was spin-coated on top of the SnO_2 ETL using a two-step spin-coating procedure, the first step at 1000 rpm for 15 seconds followed by a second step at 4000 rpm for 45 seconds. 90 µL of the mixed halide perovskite solution was used for spin coating, followed by treatment with 750 µL of diethyl ether as anti-solvent during the last 15th second of the second spin coating step. These films were then annealed at 150°C on a hot plate for 15 minutes. The $MAPbI_3$ precursor solution was prepared using 159 mg of MAI and 461 mg of PbI_2 dissolved in 66 µL of DMSO and 636 µL of DMF and stirred for 1 hour. For the deposition of $MAPbI_3$ perovskite active layer, the precursor solution was spin-coated onto the glass/ITO/SnO_2 substrate at 4000 rpm for 30 s, a diethyl ether (DEE) anti-solvent washing was carried out at the first 7th second of spin-coating process. The spin-coated perovskite films were then annealed under vacuum at 100°C for 1 min followed by 2 mins annealing in ambient N_2 inside a N_2 glovebox.

For the deposition of the HTL, 55 µL of a Spiro-OMeTAD solution [(72.3 mg of Spiro-OMeTAD, 28.8 µL of tBP, 17.5 µL of a Li-TFSI solution (520 mg Li-TFSI in 1 mL acetonitrile) and 29 µL of a FK-209 solution (300 mg FK-209 in 1 mL acetonitrile)] in 1 mL chlorobenzene was spin coated at 4000 rpm for 30 seconds on the perovskite active layer. Before spin coating, the individual solutions for HTL were thoroughly mixed using the vortex mixer. The perovskite and HTL weighing, precursor solution preparation, stirring, perovskite active layer and HTL spin coating were undertaken in a nitrogen-filled glove box with relative humidity <15%. The glass/ITO/SnO_2/perovskite/Spiro-OMeTAD structures were wrapped in Aluminum foil and left overnight in a desiccator at room temperature for oxygen doping of Spiro-OMeTAD. Finally, a 60 nm thick Au electrode was thermally evaporated (chamber pressure $3x10^{-6}$ mbar) on top of the HTM to complete the perovskite solar cell device. An aperture mask with area 0.05 cm^2 was employed to determine the effective active area of the device.

For p-i-n $MAPbI_3$ devices, 1.4 mg/mL HTL poly-TPD was dissolved in 1 mL chlorobenzene and stirred continuously for 4 hours under room temperature, Poly-TPD was spin-coated onto the cleaned

ITO substrate at 6000 rpm for 30 s. 1 mg/mL PFN-P1 was dissolved in 995 μL methanol, stirring for 2 hours under 60 °C, and then 5 μL aceticacid was added and stirred for another 2 hours under 60 °C. 100 μL of PFN-P1 was spin coated on top of poly-TPD at 3000 rpm for 30 s. The perovskite film was spin-coated using the same condition as n-i-p $MAPbI_3$ devices. For ETL deposition, 13 mg $PC_{60}BM$ was dissolved in 1 mL chlorobenzene and stirred for 4 hours under 60°C, 100 μL of the PC60BM solution was spin-coated onto the perovskite layer at 1000 rpm for 1 min. To prepare BCP solution, 0.5 mg BCP was dissolved in 1 mL anhydrous ethanol, stirred for 4 hours under room temperature and 100 μL of the BCP solution was spin-coated at 4000 rpm for 30 s. 100 nm Ag electrode was then deposited on the top of BCP by thermal evaporation.

(b) Characterisation of perovskite solar cells

For all indoor illumination measurements, a 'warm white' LED bulb with colour temperature 2700 K was used. The distance from the bulb to the photovoltaic sample being measured is adjustable and it was set such that the intensity was 0.3 mW cm^{-2} each time. The irradiance level was measured using Optometer P9710. The bulb was fixed in a dark box to help reduce background light entering the box. For 1 Sun measurement, a solar simulator was used with Xenon Arc lamp (150 W, 50 x 50 mm, Class AAA, Sciencetech Model No. Sci-Sun-150) and intensity was set to 100 mW cm^{-2} (AM 1.5G or 1 Sun). The light intensity was calibrated using a standard silicon solar cell (ORIEL® PV Reference Cell System; Model number 91150V, certified by NREL) before undertaking J-V measurements. The J-V characteristics were measured using the Ossila Source Measure Unit (SMU) and a Ossila Solar Cell IV software. The devices were under dark before implementing the J-V scans. In the case of pre-bias, the devices were applied a voltage of -1.2 V before undertaking the J-V scan. Each device was measured for a voltage range of -0.1 V to 1.5 V, with a voltage settling time of 0.2 s. The selected voltage increments were 0.01, 0.05 & 0.15 V for obtaining three different scan rates of 0.59, 0.20 and 0.04 V/s. The MPPT measurements were also undertaken using the same Ossila J-V measurement set up. The light intensity dependent J-V characteristics of the perovskite photovoltaic devices were performed using all-in-one characterization platform, Paios, Fluxim AG, Switzerland.

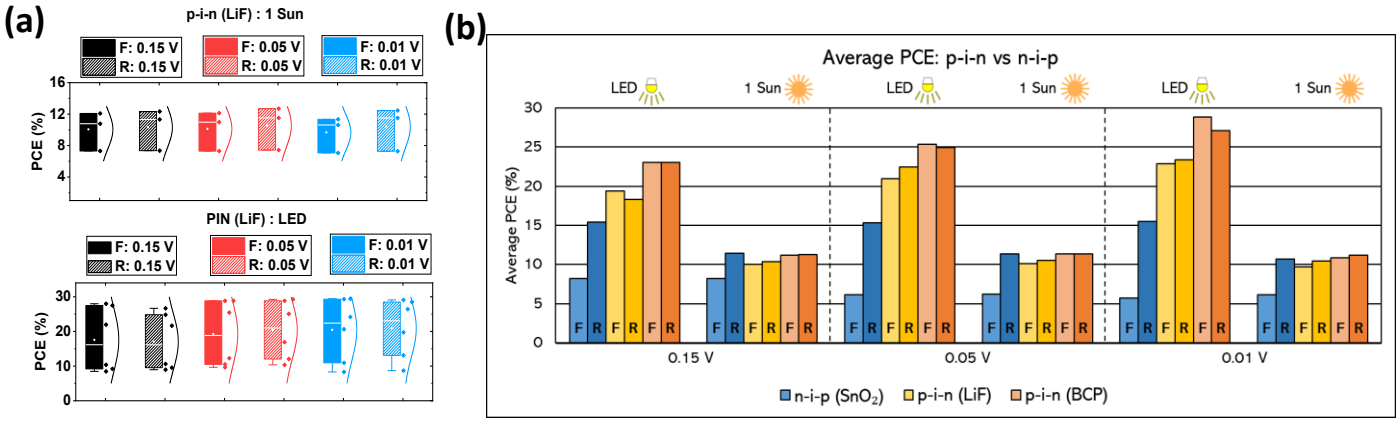

Figure S1: (a) PCE values of p-i-n devices with LiF buffer layer as a function of scan rate under 1 Sun illumination and indoor LED illumination. (b) Average PCE values of p-i-n and n-i-p devices as a function of scan rate under 1 Sun and indoor LED illumination.

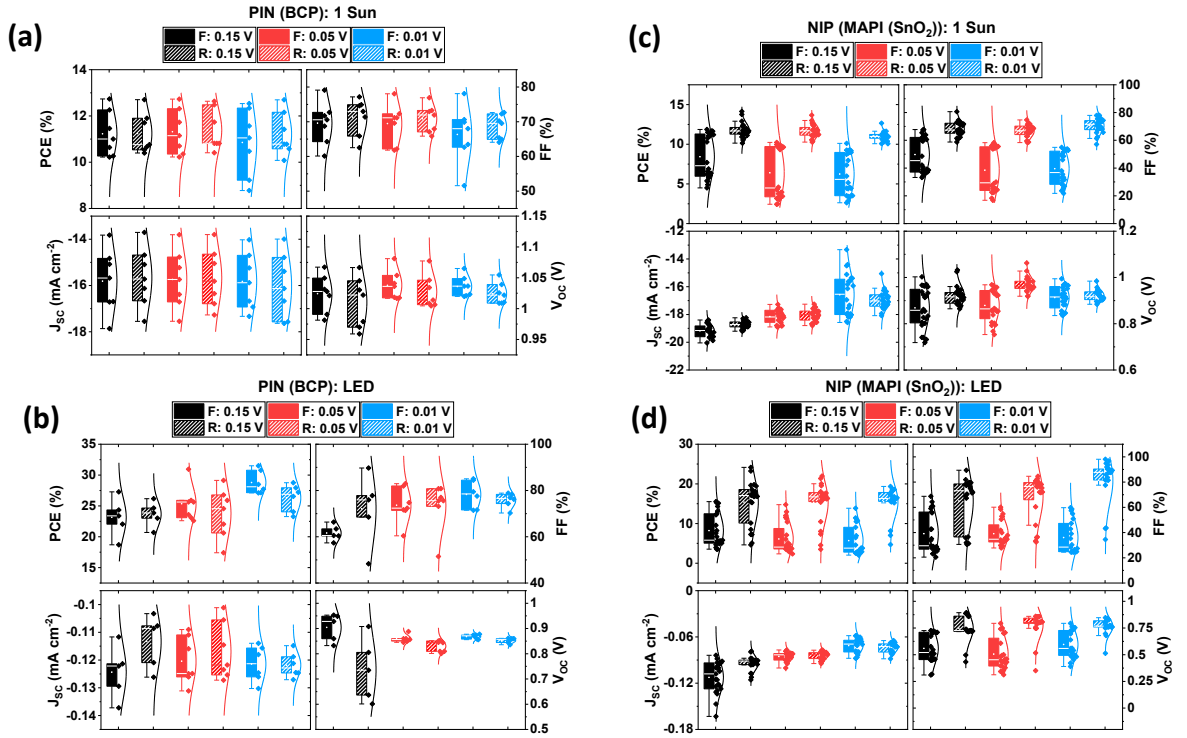

Figure S2: (a) The variation of PCE and photovoltaic performance parameters of FF, Voc and Jsc in p-i-n (BCP) devices as a function of scan rate under 1 Sun illumination. (b) The variation of PCE and photovoltaic performance parameters of FF, Voc and Jsc in p-i-n (BCP) devices as a function of scan rate under indoor LED illumination. (c) The variation of PCE and photovoltaic performance parameters of FF, Voc and Jsc in n-i-p devices as a function of scan rate under 1 Sun illumination. (d) The variation of PCE and photovoltaic performance parameters of FF, Voc and Jsc in n-i-p devices as a function of scan rate under indoor LED illumination

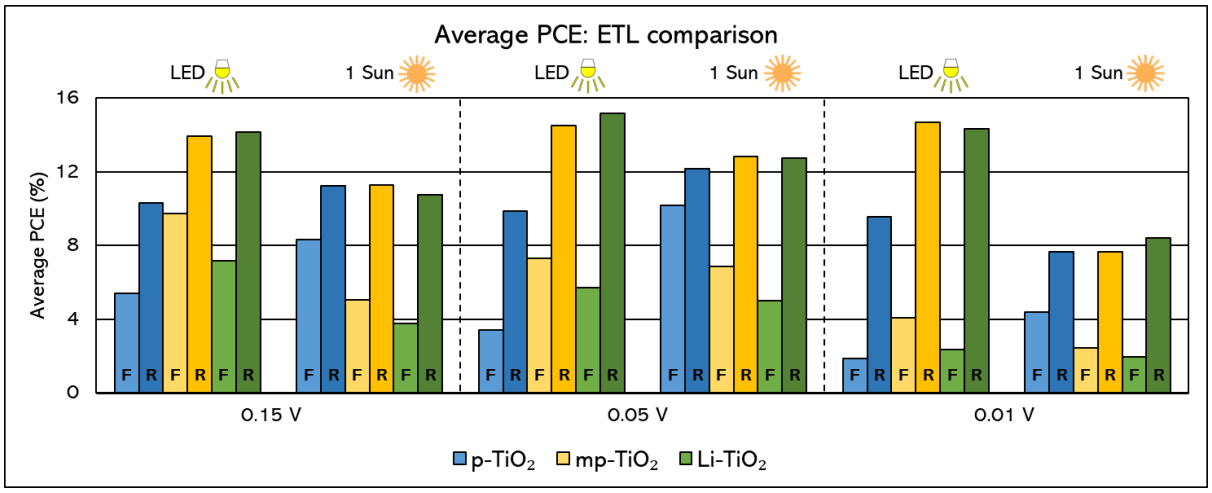

Figure S3: Comparison of the average PCE values of the n-i-p $MAPbI_3$ devices with different TiO_2 based ETLs under 1 Sun and indoor LED illumination conditions as a function of scan rates.

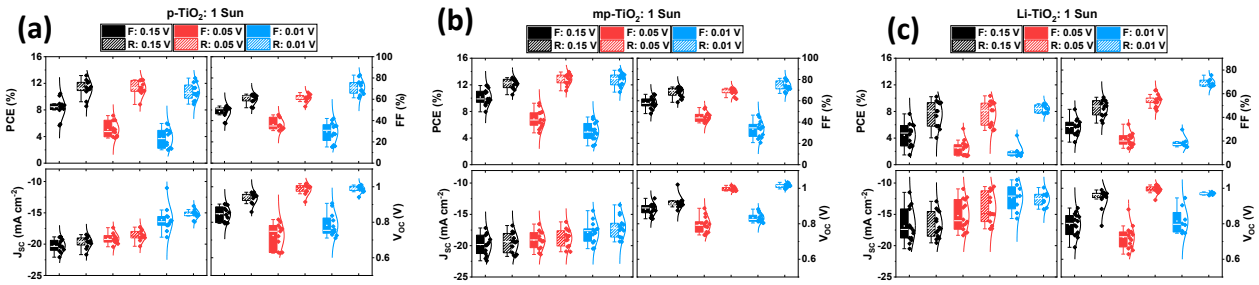

Figure S4: (a) PCE, FF, Voc and Jsc variation as a function of scan rate under 1 Sun for p-TiO_2 ETL based n-i-p $MAPbI_3$ devices. (b) PCE, FF, Voc and Jsc variation as a function of scan rate under 1 Sun for mp-TiO_2 ETL based n-i-p $MAPbI_3$ devices. (c) PCE, FF, Voc and Jsc variation as a function of scan rate under 1 Sun for Li-TiO_2 ETL based n-i-p $MAPbI_3$ devices.

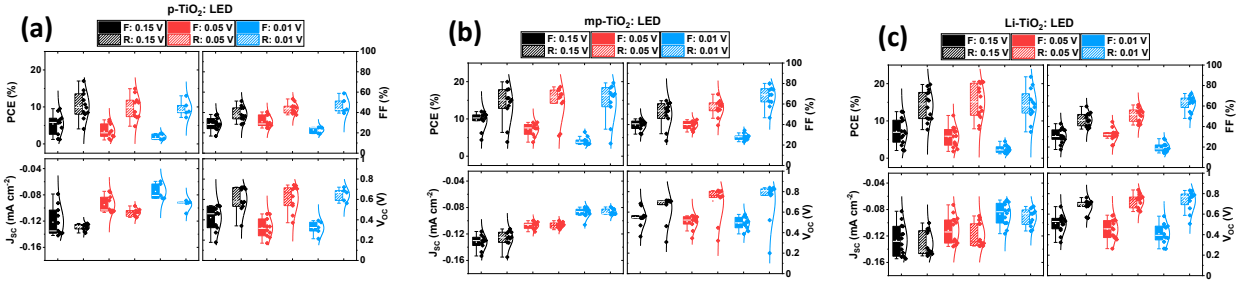

Figure S5: (a) PCE, FF, Voc and Jsc variation as a function of scan rate under indoor LED illumination for p-TiO_2 ETL based n-i-p $MAPbI_3$ devices. (b) PCE, FF, Voc and Jsc variation as a function of scan rate under indoor LED illumination for mp-TiO_2 ETL based n-i-p $MAPbI_3$ devices. (c) PCE, FF, Voc and Jsc variation as a function of scan rate under indoor LED illumination for Li-TiO_2 ETL based n-i-p $MAPbI_3$ devices.

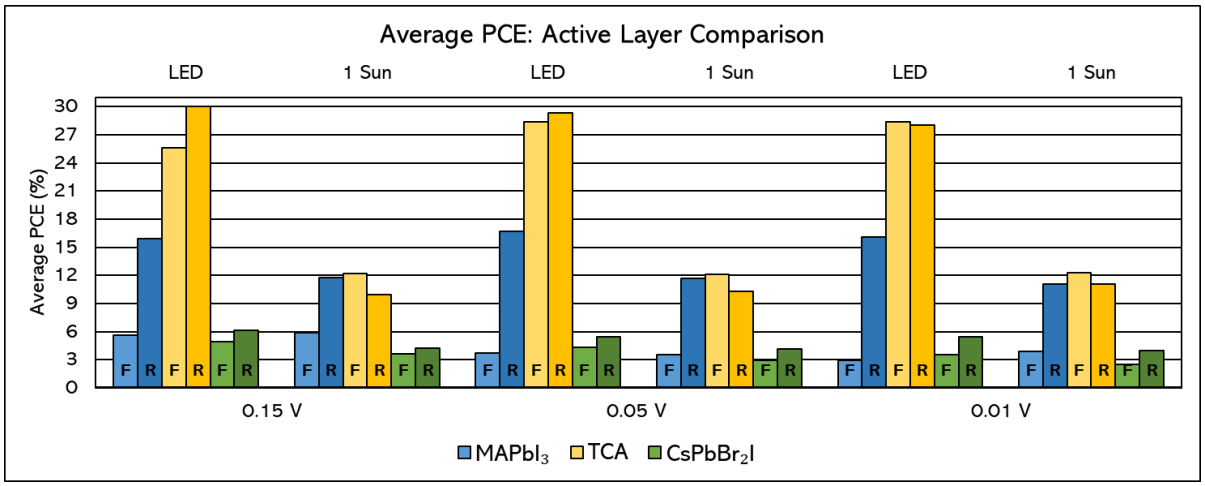

Figure S6: Average PCE for forward and reverse scan under LED and 1 Sun at three different scan rates for the devices based on the three different active layers, $MAPbI_3$, TCA and $CsPbBr_2I$.

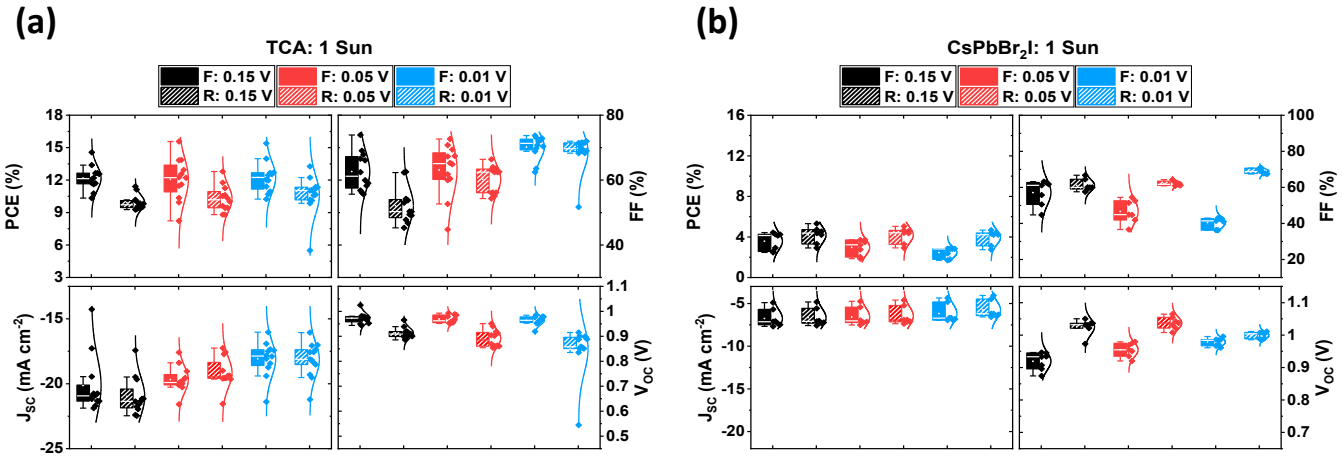

Figure S7: (a) PCE, FF, Voc and Jsc variation as a function of scan rate under 1 Sun illumination for n-i-p TCA devices. (b) PCE, FF, Voc and Jsc variation as a function of scan rate under 1 Sun illumination for n-i-p CsPbBr2I devices.

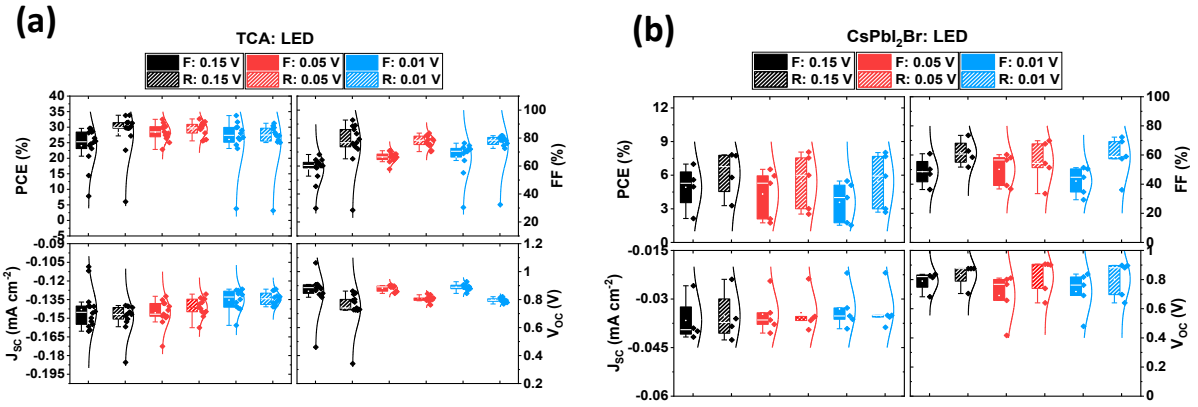

Figure S8: (a) PCE, FF, Voc and Jsc variation as a function of scan rate under indoor LED illumination for n-i-p TCA devices. (b) PCE, FF, Voc and Jsc variation as a function of scan rate under indoor LED illumination for n-i-p $CsPbBr_2I$ devices.

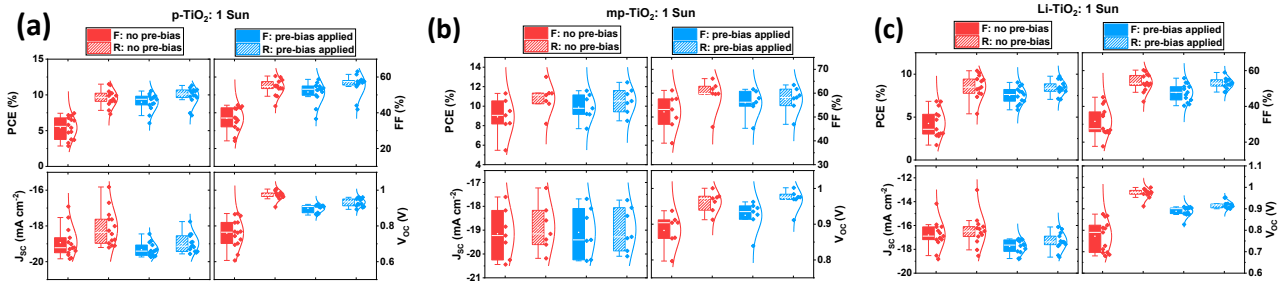

Figure S9: Effect of pre-bias on the PCE and the photovoltaic performance parameters under 1 Sun illumination for forward and reverse scan. The n-i-p device architecture uses different types of TiO_2 ETLs; (a) p-TiO_2, (b) mp-TiO_2, (c) Li-TiO_2. The voltage increment considered here is 0.15 V.

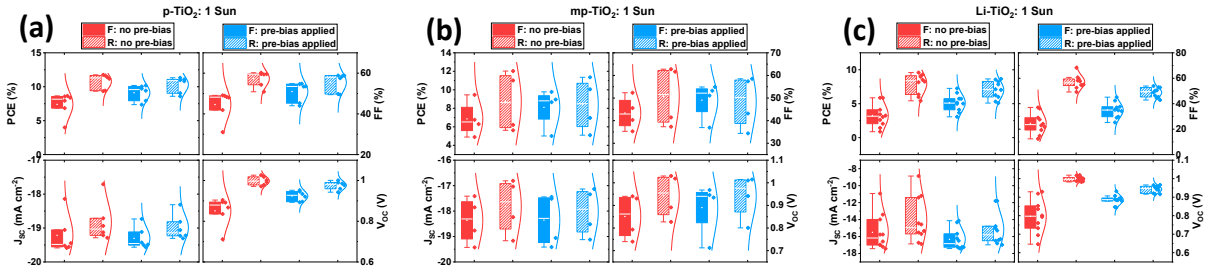

Figure S10: Effect of pre-bias on the PCE and the photovoltaic performance parameters under 1 Sun illumination for forward and reverse scan. The n-i-p device architecture uses different types of TiO_2 ETLs; (a) p-TiO_2, (b) mp-TiO_2, (c) Li-TiO_2. The voltage increment considered here is 0.05 V.

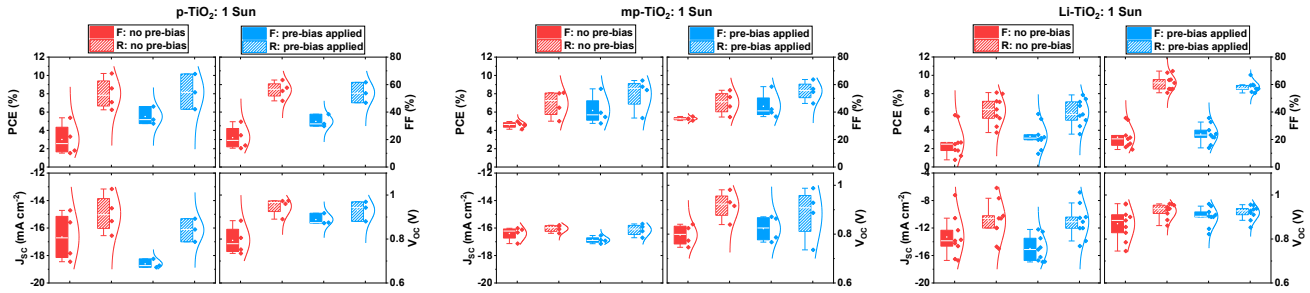

Figure S11: Effect of pre-bias on the PCE and the photovoltaic performance parameters under 1 Sun illumination for forward and reverse scan. The n-i-p device architecture uses different types of TiO_2 ETLs; (a) p-TiO_2, (b) mp-TiO_2, (c) Li-TiO_2. The voltage increment considered here is 0.01 V.

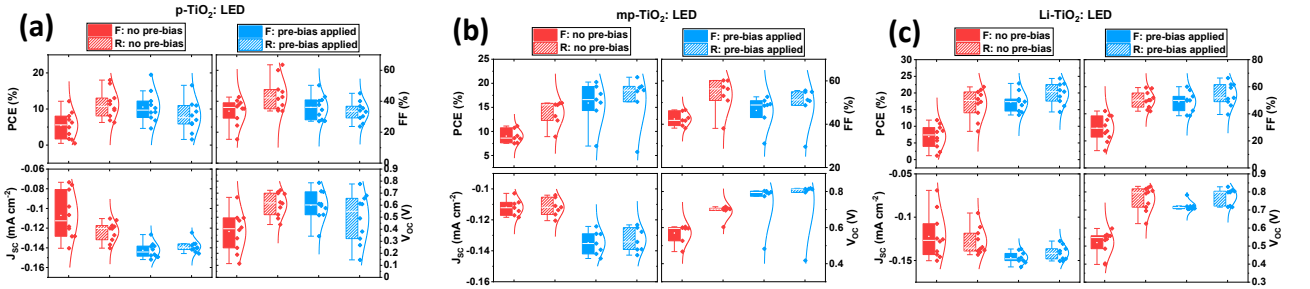

Figure S12: Effect of pre-bias on the PCE and the photovoltaic performance parameters under indoor LED illumination for forward and reverse scan. The n-i-p device architecture uses different types of TiO_2 ETLs; (a) p-TiO_2, (b) mp-TiO_2, (c) Li-TiO_2. The voltage increment considered here is 0.15 V.

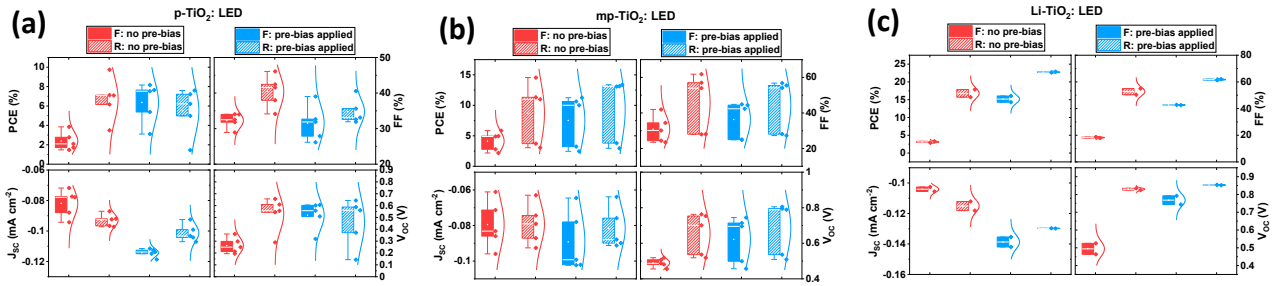

Figure S13: Effect of pre-bias on the PCE and the photovoltaic performance parameters under indoor LED illumination for forward and reverse scan. The n-i-p device architecture uses different types of TiO_2 ETLs; (a) p-TiO_2, (b) mp-TiO_2, (c) Li-TiO_2. The voltage increment considered here is 0.05 V.

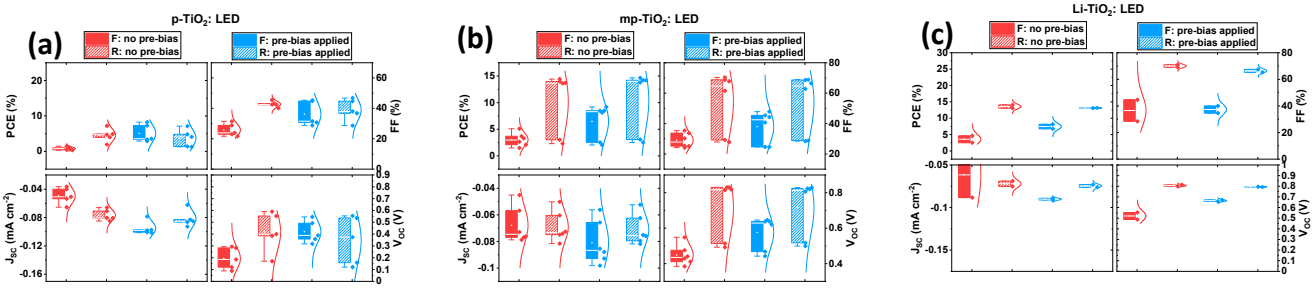

Figure S14: Effect of pre-bias on the PCE and the photovoltaic performance parameters under indoor LED illumination for forward and reverse scan. The n-i-p device architecture uses different types of TiO_2 ETLs; (a) p-TiO_2, (b) mp-TiO_2, (c) Li-TiO_2. The voltage increment considered here is 0.01 V.

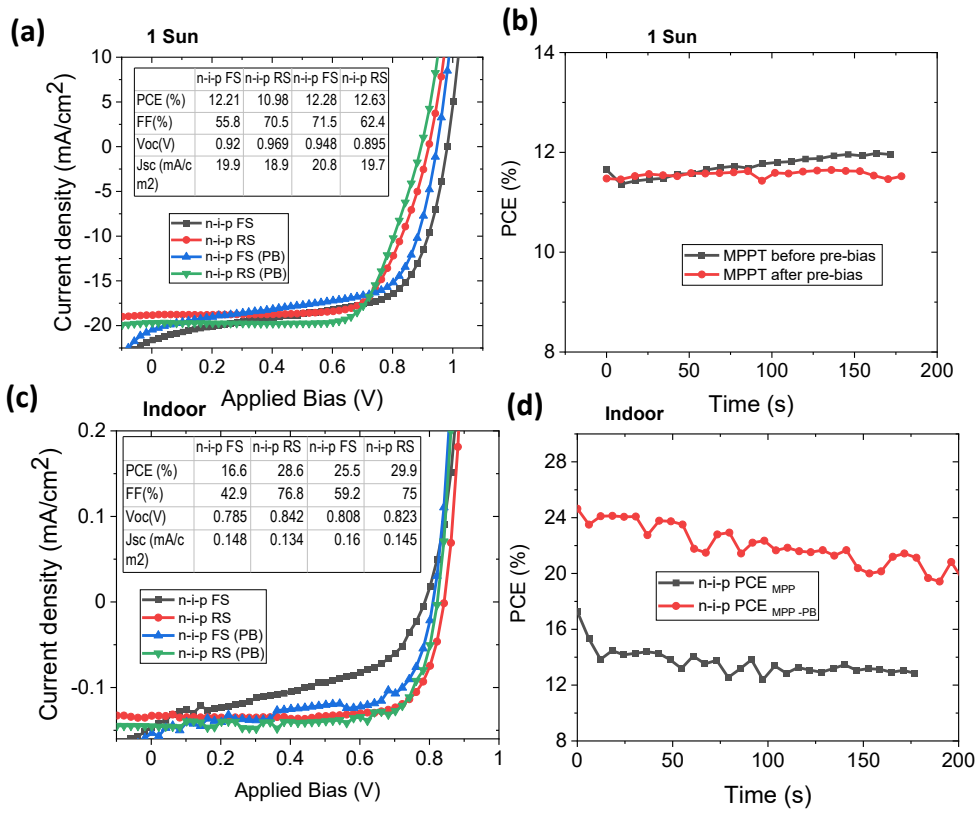

	n-i-p FS	n-i-p RS	n-i-p FS	n-i-p RS
PCE (%)	12.21	10.98	12.28	12.63
FF(%)	55.8	70.5	71.5	62.4
Voc(V)	0.92	0.969	0.948	0.895
Jsc (mA/cm2)	19.9	18.9	20.8	19.7

	n-i-p FS	n-i-p RS	n-i-p FS	n-i-p RS
PCE (%)	16.6	28.6	25.5	29.9
FF(%)	42.9	76.8	59.2	75
Voc(V)	0.785	0.842	0.808	0.823
Jsc (mA/cm2)	0.148	0.134	0.16	0.145

Figure S15: (a) & (b) Effect of pre-bias on n-i-p $MAPbI_3$ devices as reflected in the J-V curves and MPPT measurements under 1 Sun illumination, respectively. (c) & (d) Effect of pre-bias on n-i-p $MAPbI_3$ devices reflected in the J-V curves and MPPT measurements for LED indoor illumination, respectively.